Visual Neuroscience (2001), **18**, 961–972. Printed in the USA.

DOI: 10.1017.S095252380118613X

Transmission of spatial information in S-cone pathways

ANDREW B. METHA[1] AND PETER LENNIE*

Center for Visual Science, University of Rochester, Rochester, New York

(RECEIVED July 17, 2001; ACCEPTED November 2, 2001)

Abstract

The mosaics of S-cones and the neurons to which they are connected are relatively well characterized, so the S-cone system is a good vehicle for exploring how the sampling of the retinal image controls visual performance. We used an interferometer to measure the grating acuity of the S-cone system in the fovea and at a range of eccentricities out to 20 deg. We also developed a simple model observer that, by assuming only that cone pathways are noisy and that signals are subject to eccentricity-dependent postreceptoral pooling, predicts the measured acuities from the sampling properties of the S-cone mosaic. The amount of pooling required to explain performance is consistent with that suggested by anatomical and physiological measurements.

Keywords: S-cones, Aliasing, Acuity, Spatial frequency

Introduction

We want to understand how the known distribution of cones can account for psychophysical performance in spatial resolution tasks. Because we know a great deal more about the spatial organization of short-wavelength-sensitive (S) cone pathways than we do about the organization of other pathways, the S-cone system provides a good vehicle for exploring general questions about the relationship between the sampling properties of mosaics and perceptual performance. In principle, this should be straightforward because the S-cones and the neurons known to convey their signals are clearly identified and sparse, so the fine structures of their mosaics are easily discerned anatomically. S-cones can be identified unambiguously in flat mounts of both macaque monkey (McCrane et al., 1983) and human (Curcio et al., 1991) retinas. They are connected to a distinct population of bipolar cells (Kouyama & Marshak, 1992), and in turn to at least one special population of ganglion cells (the small bistratified ganglion cells) that provides the substrate of the "blue-on, yellow-off" color-opponent pathway (Dacey & Lee, 1994). "Blue-off, yellow-on" neurons are much less frequently encountered (de Monasterio & Gouras, 1975; Derrington et al., 1984; Valberg et al., 1986), and no anatomical substrate has yet been identified.

Spatial sampling by the S-cone system in the normal fovea has been explored before (Williams & Collier, 1983), but has not been characterized at a range of eccentricities that would permit performance to be systematically related to the sampling properties of the anatomical mosaics. Moreover, because the mosaics of S-cones, bipolar cells, and ganglion cells are not perfectly crystalline, and because we do not know much about how irregularly spaced sampling elements should affect the representation of spatial structure around the sampling limits of mosaics, no simple analysis exists to connect psychophysical performance with the anatomical observations.

In this paper, we describe psychophysical measurements of the acuity of the S-cone system at a range of eccentricities along the horizontal meridian in nasal and temporal retina, obtained using interference fringes formed directly on the retina. We then develop a simple model that predicts acuities from the sampling properties of the constituent mosaics of the S-cone system. This model assumes only that noise is added to the cone signals and that as eccentricity grows these signals are increasingly pooled by postreceptoral mechanisms.

Methods

Apparatus

Fig. 1 shows how sinusoidal gratings were formed directly on the retina by a laser interferometer. We used a dual polarization interferometer designed and built by Nobu Sekiguchi and David Williams, and described fully in Sekiguchi et al. (1993). The instrument was mounted on an air-cushioned optical table, as schematized in Fig. 1.

Coherent, polarized 441.6-nm light is produced by a Liconix 10 mW Helium-Cadmium continuous gas laser. A half-wave plate (HP) and a linear polarizer (LP1) together act to control the intensity of the beam, and to polarize light at 45 deg from vertical. The polarizing beam splitter (PB1) transmits the vertically polarized component of this light to the first of two identical acousto-optic modulators (AOM1), and reflects an equal amount of horizontally polarized light to AOM2. A 500-Hz square-wave

Address correspondence and reprint requests to: Andrew B. Metha, Department of Optometry and Vision Sciences, The University of Melbourne, Corner Cardigan and Keppel Streets, Carlton, 3052, Australia.

*Present address of Peter Lennie: Center for Neural Science, New York University, 4 Washington Place, New York, NY 10003, USA.

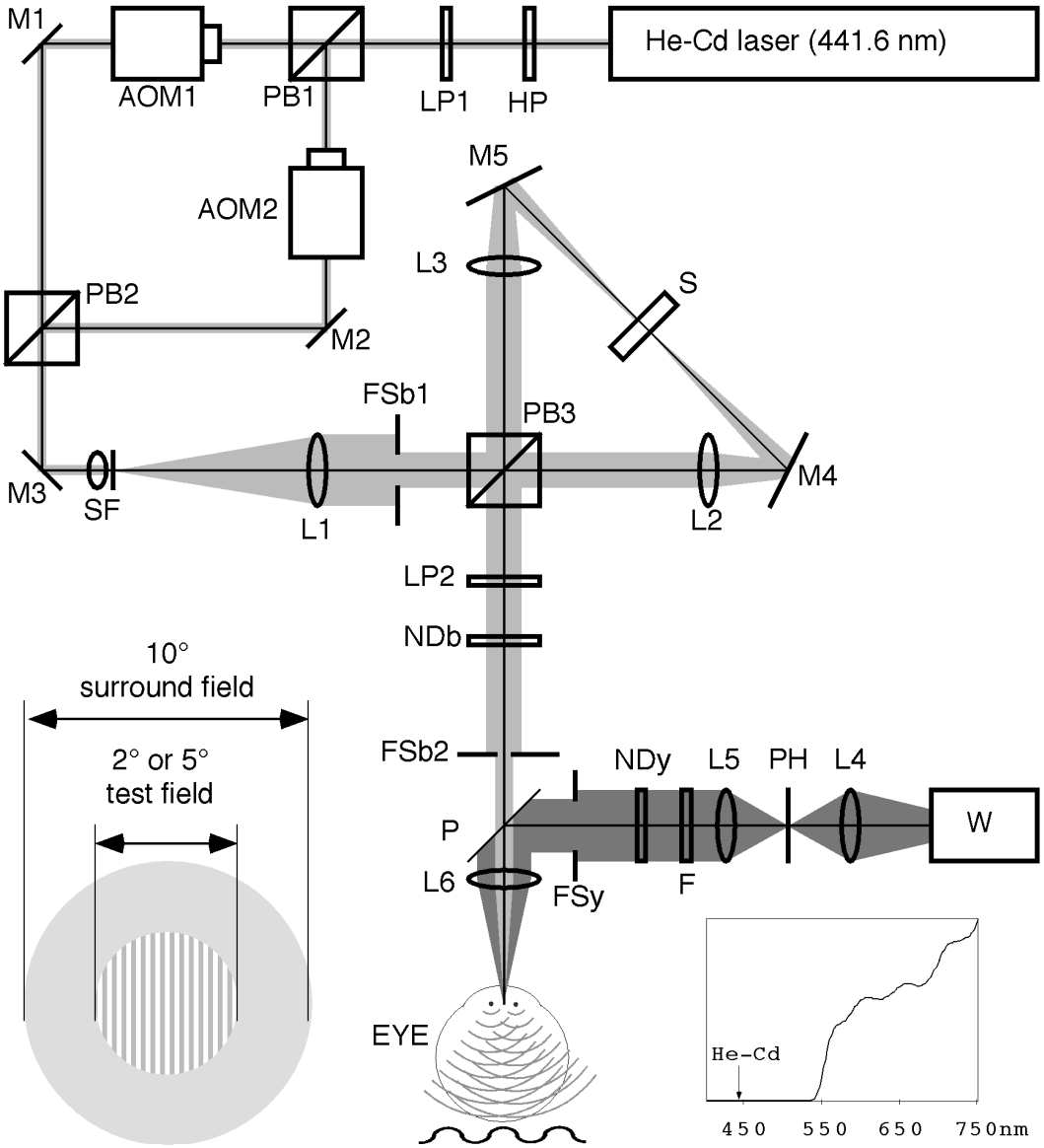

Fig. 1. Two-channel Maxwellian view apparatus used to deliver high contrast S-cone isolating gratings. One path incorporates a 441.6-nm helium–cadmium laser interferometer to generate gratings, and a second path introduces a bright yellow adapting light to selectively reduce responses from L- and M-cones. See text for details.

current applied to each AOM chops the light into 1-ms pulses. The relative phases of these pulse trains in the two AOMs determines the contrast of the resulting interference fringe: when the pulses are exactly in phase (overlap fully) the two beams interact fully to produce a grating of unit contrast; when the pulses are out of phase, no interference occurs and the contrast is zero. Mean retinal illuminance remains constant. Using orthogonally polarized beams in this manner allows the twin light paths to share almost all optical components in the instrument, and minimizes fringe distortion from mechanical instability. The two beams are brought into exact register by mirrors M1-2 and polarizing beam splitter PB2, reflected by mirror M3 into a spatial filter (SF—a microscope objective held in reverse). This focuses the beams to pass through a 5-μm aperture that becomes a point source of light for the next stage of the interferometer.

Lens L1 collimates light from SF, and the expanded beams pass through the circular field stop FSb1, after which they are divided by polarizing beam splitter PB3. The transmitted vertically polarized component is focused by lens L2 to a point image in the center of the flat glass slab S. Similarly, the horizontally polarized beam is reflected by PB3 and is focused by L3 into the center of a glass slab S, which is secured in a two-axis gimbal-mount that permits its rotation about two orthogonal axes under computer-driven stepper-motor control. When S is perpendicular to the optical axis of the apparatus, the two point images will be coincident. Rotations of S from perpendicularity cause equal and opposite displacements of the point images away from the optical axis. Further optics make these two point images conjugate with the observer's pupil plane, so that rotations of S control the orientation and spatial frequency of the interference grating on the retina without the need for realigning the observer's eye. From S, the beams are again collimated and recombined by PB3 before passing through the linear polarizer PL2, whose axis of extinction is held at 45 deg with respect to both beams so as to pass equal amounts of the two

components, rendering these in the same plane of polarization and thus allowing interference. The intensity of the laser light can be attenuated by placing neutral density filters at NDb. The beams pass undeviated through the field stop FSb2 and thin glass pellicle P to the Maxwellian lens L6, which focuses the two point images formed at S into the observer's entrance pupil plane. The diameter of the circular field stop FSb2 is variable and its position is conjugate with the observer's retina, allowing control over the spatial extent of the retinal interference grating.

A concentric background field is introduced into the optical path by the pellicle P. The light source is a heat-filtered tungsten lamp W, the filament of which is focused by lens L4 onto a pinhole PH to create a bright point source. This is collimated by lens L5 and rendered yellow by filter F, which has the transmission characteristic shown in the inset of Fig. 1. Background illuminance is controlled in discrete steps by calibrated ND filters at position NDy, while its size, always 10 deg, is controlled by the retinally conjugate field stop FSy. The Maxwellian lens L6 focuses this background light to a point source (diameter $\approx$ 1 mm) in the observer's entrance pupil, between the two point sources from the interferometer. The intensity and spectral composition of the lights were measured in the entrance pupil plane using a UDT radiometric power meter and a Photo Research PR650 spectrophotometer, respectively.

Observers and alignment

Four males with normal vision served as observers, although for only three were measurements made at a full range of retinal eccentricities. One observer (AR) wore spectacle lenses during testing.

A large cardboard screen in the plane of lens L6 masked the observer from the optical apparatus. Through this screen the end of an optic fiber could be placed to provide a fixation spot at defined positions out to 20 deg left and right on the horizontal meridian. Stimulus eccentricity was controlled by directing fixation at this small lit target, except when this would fall within the yellow background field; in this case the observer fixated a small mark on a microscope slide held in the retinal conjugate plane of FSy. The observer's head was held steady by a dental bite-bar mounted on a three-axis translating stage. This stage was adjusted for best eye alignment at each eccentricity. The eye was aligned axially by a knife-edge test with the top of the pupil, so that the point images were formed in the pupil plane. To align the eye vertically and horizontally, the observer exploited the Stiles-Crawford effect to maximize the apparent brightness of the stimulus field. Centered point images were not critically important because of the small image sizes and low spatial-frequency range under investigation: for example, a 20 cycle/deg stimulus required the interferometer beams to be separated by approximately 0.5 mm. Nevertheless, ophthalmic tropicamide solution was instilled to dilate the pupil and paralyze accommodation before testing. The fellow eye was occluded with a translucent cover.

Psychophysical Procedure

To establish the highest spatial-frequency gratings that the observer could detect and correctly identify, we used a 2×2-interval forced-choice procedure. Each trial consisted of two 500-ms intervals (defined by tones), separated by 500 ms. In one interval, randomly chosen from trial to trial, the observer was presented with an interference grating, randomly vertical or horizontal and of full contrast, while in the other interval the contrast was zero. The transition between full and zero contrast was made by adjusting the AOM pulse overlap as described above; mean luminance remained constant, as did the position of the slab that controlled fringe orientation and spatial frequency. After each trial, observers indicated by successive button presses whether a grating pattern appeared in the first or second interval (detection question), and then whether the pattern was horizontal or vertical (orientation identification question). Auditory feedback was given immediately after the detection response but because we were interested in the possibility of orientation reversals generated by aliasing (Coletta & Williams, 1987), no feedback was supplied after the identification response. In addition, because aliasing can lead to detection acuity being substantially better than identification acuity (Williams & Collier, 1983), four independent staircases simultaneously kept track of the stimulus spatial frequency. Two of these staircases (one for each orientation) were controlled by detection responses and the other two (again, one for each orientation) by identification responses. Sixty stimulus trials were presented for each staircase, with spatial frequency increased by 0.08 $\log_{10}$ units after a correct response, and decreased by 0.16 $\log_{10}$ units after an incorrect response. Trials from the different staircases were randomly interleaved.

S-cone isolation

The optical system presented observers with a monochromatic (441.6 nm) sinusoidal interference grating of variable illuminance, size, spatial frequency, contrast, and orientation, superimposed on a 10-deg concentric yellow background field of variable illuminance (see Fig. 1, inset). The test grating was free of chromatic aberration, and contrast was compromised neither by the optics of the eye, nor by diffraction effects. The yellow background light lowered selectively the L- and M-cone contrast generated by the 441.6-nm laser interference pattern, while leaving the S-cone contrast high. When background illuminance is low and the L- and M-cone contrasts are sufficiently high, acuity will be mediated by the spatially dense array of L- and M-cones, and will therefore be high; when background illuminance is raised and L- and M-cone contrasts drop below threshold, grating visibility is determined by the spatially less dense S-cone pathway, and acuity should drop abruptly. By adjusting the illuminance of the yellow background light, we can find a level at which L- and M-cone contrasts in the image are comfortably below threshold while the S-cone contrast is high, and thereby isolate the S-cone pathway as the determinant of spatial acuity.

To find the best background for S-cone isolation, we made preliminary measurements in the fovea using a circular 2-deg grating field embedded in the center of the 10-deg yellow background field. Using calibrated ND filters inserted in the background path (Fig. 1; NDy), we explored a 2.5 $\log_{10}$ unit range of field illuminances in 0.5 $\log_{10}$ unit steps ranging from 2.7 $\log_{10}$ to 5.2 $\log_{10}$ Td. Each experimental run at a different level of yellow light consisted of 240 trials, and lasted 15–20 min, depending on how quickly observers responded. We constructed psychometric functions for both detection and orientation identification, independently for each orientation. In general, performance on neither task depended on stimulus orientation, so for both detection and identification we pooled the data for vertical and horizontal gratings.

Analysis and results

Psychometric functions

Fig. 2 shows sample psychometric functions plotting performance against log spatial frequency. Open squares show performance on the detection task; filled circles show performance on the orientation identification task. The smooth curves are base-2 Weibull functions falling smoothly from 100% at low spatial frequencies to chance levels (50%) as spatial frequency increases. The spatial frequency for 75% correct was taken as the threshold acuity. The standard deviation of performance at each spatial frequency was estimated from the binomial distribution (Macmillan & Creelman, 1991). This enables us to fit the data by minimizing the sum of squared normalized errors between the data and the function. The value of this sum (chi square) characterized goodness of fit. If there was a significant error in the fit ($P < 0.05$) the experimental run was repeated. Another benefit of this analysis is that the reliability of the 75% threshold can be estimated with a standard deviation measure given by the curve fit.

The separation of detection and identification curves in Fig. 2 presumably reflects aliasing, which prevents faithful representation of the stimulus but does not remove signals that enable it to be distinguished from a blank field (Williams & Collier, 1983). This figure shows that observer SD's detection acuity exceeds his orientation identification acuity by almost a factor of four; indeed his detection acuity is unusually good, being almost twice that of any observer in Williams and Collier's (1983) study. Detection and identification thresholds were more similar for other observers, and either measure could be used to determine the conditions under which S-cones were isolated. Fig. 3 shows, for two observers, how each acuity measure for foveally viewed patterns varied with the illuminance of the yellow background. Both identification and detection acuities were high when the background illuminance was low. Under these conditions gratings appeared as crisply defined stripes, even at the highest spatial frequencies. The numbers next to each datum in the right-hand panel indicate the L-, M-, and S-cone contrast calculated for each background light condition, assuming the Smith-Pokorny fundamentals (Smith & Pokorny, 1975). High acuity is associated with high L- and M-cone contrasts. With increasing background illuminance, L- and M-cone contrasts fall much more rapidly than does S-cone contrast, and so does acuity, which by either measure becomes asymptotically low between 4.7–5.2 $\log_{10}$ Td, corresponding to L-, M-, and S-contrasts of 0.001, 0.004, and 0.938, respectively. At these levels we assume that the in-phase L- and M-cone contrasts are too low to contribute to threshold, which instead must be carried by the S-cone signals alone. Under these conditions, gratings appeared distinctly different from the crisply defined stripes observed at lower background light levels. All subsequent measurements were made using a 4.9 $\log_{10}$ Td yellow background.

S-cone acuity across the retina

We used the methods described above to measure concurrently the S-cone acuities for detection and orientation identification in three observers (PL, AR, and AM) over a range of eccentricities spanning 40 deg on the horizontal meridian. For all measurements the yellow background field was fixed at 10 deg. The diameter of the monochromatic test field was 2 deg for measurements at eccentricities out to 10 deg; at greater eccentricities it was 5 deg.

Fig. 4 shows each observer's acuity for detection (open squares) and orientation identification (filled circles) as a function of eccentricity. Detection acuities are generally higher than identification acuities, but decline much less regularly with eccentricity. Best acuity of 5.8–13.9 cycle/deg at the fovea presumably reflects the fact that the 2-deg grating extended well beyond the central 0.5 deg in which there are no S-cones (Willmer & Wright, 1954; Wald, 1967; Williams et al., 1981; Catsano & Sperling, 1982), into the region of peak density at around 1 deg (de Monasterio et al., 1985; Curcio et al., 1991). Detection acuity is on average 1.5 times better than orientation identification acuity, though the gap would presumably be bigger if pupil alignment were identical for all eccentricities (see below).

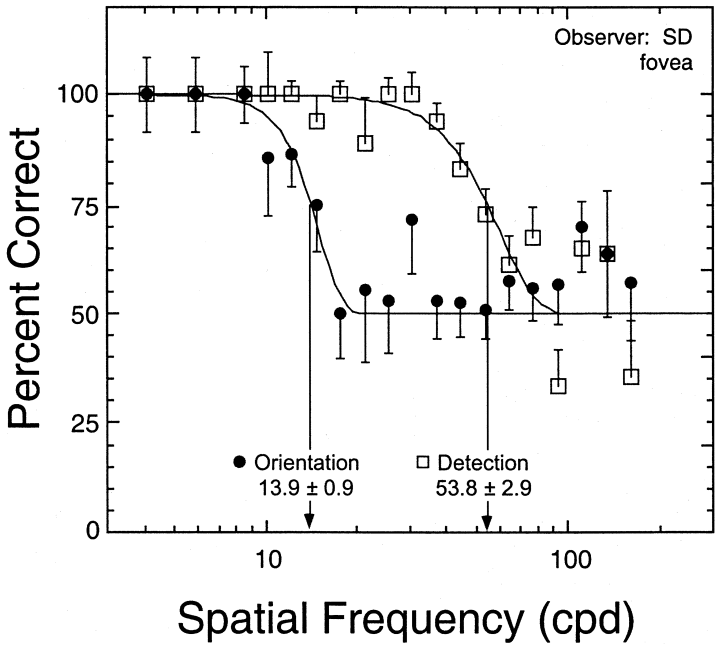

Fig. 2. Psychometric functions showing percent correct performance against log spatial frequency (cycles per degree). A 2 × 2-alternative forced-choice procedure was used. Open squares show performance on the detection task (i.e. deciding which of two intervals contained the grating). Filled circles show performance on the identification task (i.e. deciding whether the grating was vertical or horizontal). Responses controlled the spatial frequency of presented gratings according to four adaptive staircases: two tracking detection and two tracking identification. Threshold acuities were taken to be the spatial frequencies for which decisions were correct on 75% of trials.

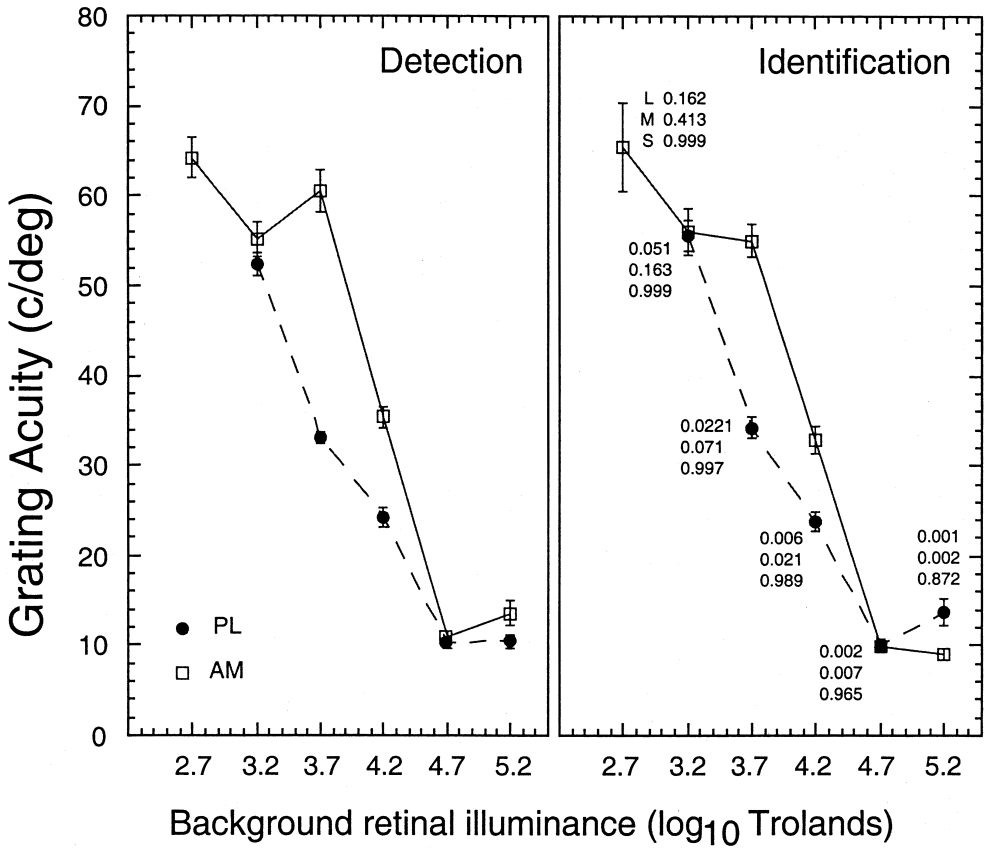

Fig. 3. Foveal detection (left) and identification (right) acuities for two observers measured over a 2.5 $\log_{10}$ unit range of yellow background illuminances. Numbers adjacent to points in the right-hand panel indicate the L-, M-, and S-cone contrasts in each background condition.

The considerable variation in detection acuity, both within and between individuals, might be related to the appearance of the stimuli under different conditions. At low spatial frequencies the stimulus looked like a regular grating with well-defined orientation (although lacking the crispness seen when it was visible to L- and M-cones at lower background illuminances). With increasing spatial frequency, the pattern appeared to scintillate and became increasingly ill-defined (splotchy) as orientation identification performance fell to chance level. Stimuli in this state resemble the laser speckle pattern when the field is blank, though the contrast and temporal characteristics are sufficiently different that the two conditions can be distinguished. At yet higher spatial frequencies, even these differences disappear, and detection performance falls to chance. The appearance of the laser speckle in both the test and blank intervals varies with the axial alignment of the observer with the optical apparatus (Williams, 1985*b*; Sekiguchi et al., 1993). Despite the use of the subjective knife-edge test to achieve a standard alignment on the entrance pupil plane, small variations in alignment at different eccentricities result in different speckle patterns that raise detection thresholds by varying amounts.

When S-cones were isolated, no observer reported seeing anything like the "zebra stripes" or Moiré patterns that characterize the appearance of very high spatial-frequency achromatic patterns in the fovea. Such patterns were however seen at high spatial frequencies with lower background illuminances that permitted grating detection by M- and L-cones. When thresholds were determined by S-cones all observers reported seeing splotchy percepts of the kind first described by Williams and Collier (1983); this was true for all eccentricities tested. Identifying the orientation of the grating then became a matter of deciding whether the splotches looked more vertical or horizontal. Moiré patterns are to be expected when a grating is undersampled by a regular photoreceptor mosaic (Williams, 1985*a*). Their absence in the present S-cone isolating experiments suggests that the S-cone mosaic is at all eccentricities too irregular to generate coherent aliases.

Fig. 5 shows identification acuity averaged from Fig. 4, together with the nominal Nyquist limit of a crystalline triangular mosaic having the mean cone spacing found by Curcio et al. (1991). This makes obvious that performance exceeds the theoretical expectation near the fovea, and falls below expectation in the periphery.

A model observer for S-cone acuity

We would like to know how well the measured psychophysical performance, and perhaps the appearance of gratings, can be predicted from the sampling properties of the mosaic of S-cones and the mosaics of bipolar and ganglion cells that receive S-cone inputs. We begin by considering the sampling properties of the mosaic of S-cones.

Previous assessments of the expected performance of this mosaic (Williams et al., 1983; Curcio et al., 1991) used the sampling theorem to estimate the theoretical resolution limit of a regular (triangular) mosaic in which cone spacing is equal to the

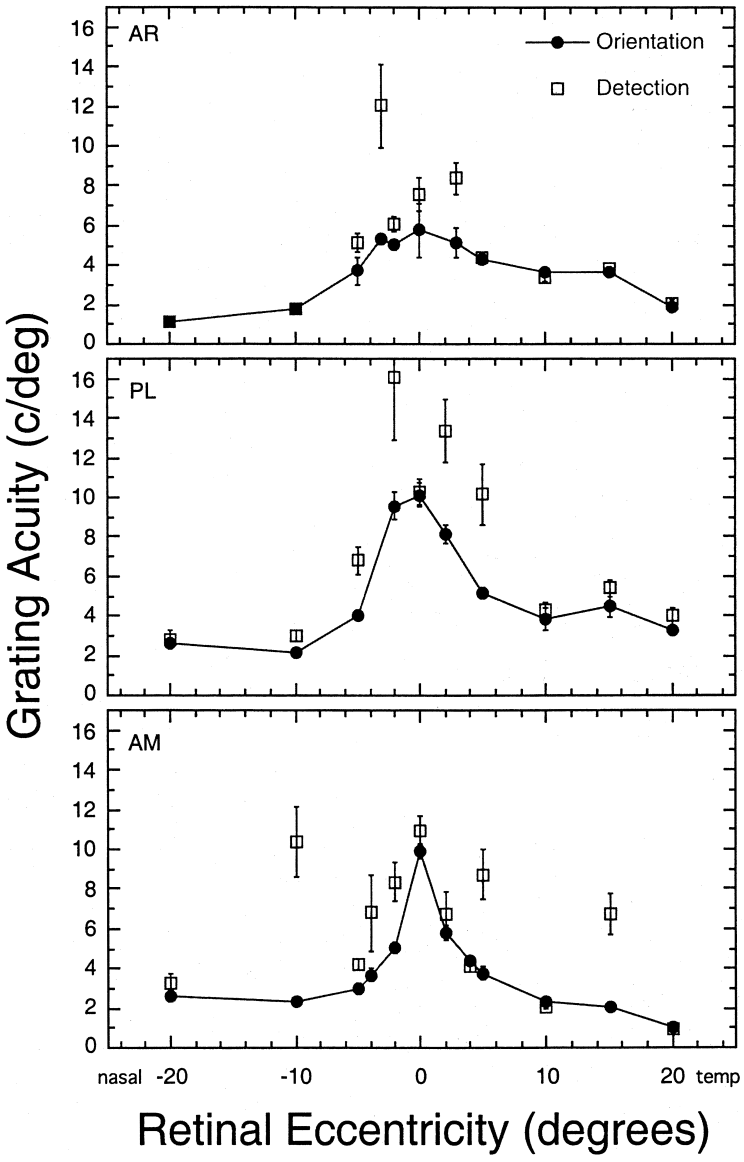

Fig. 4. Detection (filled circles) and identification (open squares) acuity of the S-cone system measured over a 40-deg range of eccentricities along the horizontal meridian, for three observers. Measurements at eccentricities $<$ 10 deg were made using a 2-deg-diameter grating patch. At greater eccentricities, a 5-deg patch was used. The shaded gray area indicates the region within which spatial aliasing occurs—when gratings can be detected but not reliably identified. For three observers, detection acuities were on average about 50% higher than identification acuities.

average observed in the real retina. This tells us the highest frequency at which the structure of a grating could be represented completely by a regular mosaic, but does not allow us to predict performance on simple tasks of the kind used here: distinguishing a grating and a uniform field, or two gratings that differ in orientation by 90 deg. Very little information will be needed for reliable detection, and not much more for reliable discrimination, so even a completely regular mosaic will be able to convey something about the structure of gratings at spatial frequencies too high to permit a complete representation. This "supra-Nyquist resolution" has been characterized by Williams and Coletta (1987). Beyond this, the irregular placement of cones in the mosaic brings about a graceful rather than abrupt degradation of capacity to reconstruct gratings of spatial frequencies above the nominal sampling limit, because the signal that would form the low-frequency alias is distributed as broadband noise (Yellott, 1982).

To predict performance, we need a more fully developed model of how an observer might detect or distinguish the signals that arise from an irregular mosaic when gratings of a given spatial frequency fall on it. We have therefore constructed a model observer whose task is to examine the signals that arise in a mosaic of S-cones and to distinguish those arising under different conditions: a grating versus a spatially uniform field, and a vertical grating versus a horizontal one.

We begin by synthesizing five mosaics of 1600 S-cones, each having the statistical structure found in the primate retina. To do this, we use the "elastic ball" method developed by Shapiro et al. (1985). By this method, a mosaic is created by sequentially adding cones in randomly chosen positions, with the constraint that no new cone may ever lie within a specified distance from an existing cone, and that beyond this forbidden region the chance of a cone being admitted to the mosaic grows with distance. With appropriate choice of probability curve that defines this outer "soft shell", the method generates mosaics whose statistics (of distances between Voronoi neighbors and central angles of Voronoi regions) describe real S-cone mosaics in macaque (Shapiro et al., 1985) and ground squirrel (Galli-Resta et al., 1999). S-cone distributions differ in the human and macaque foveas (Bumsted & Hendrickson,

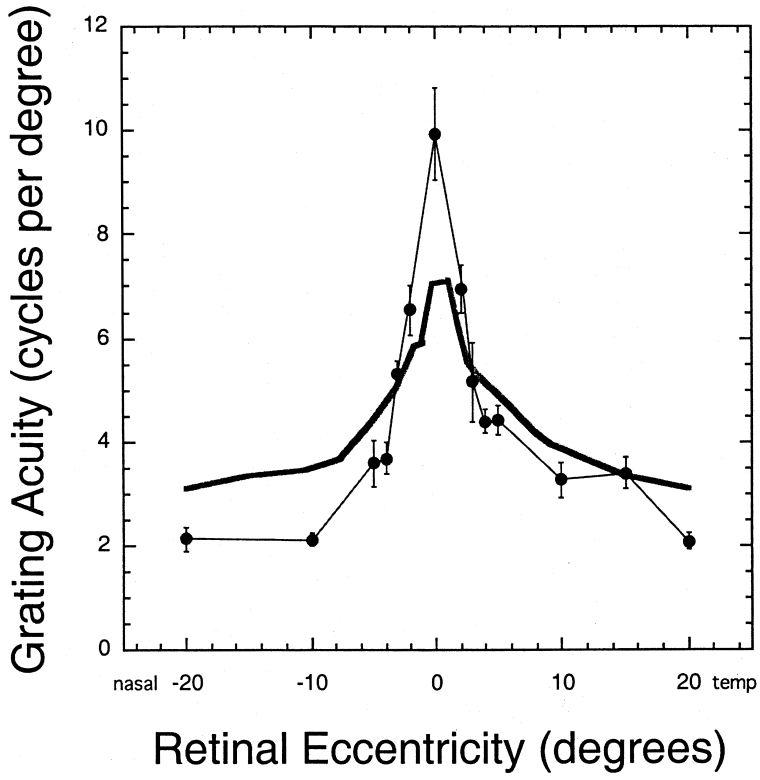

Fig. 5. Average identification acuity (filled circles) for all observers at all retinal locations that measurements were made. Vertical bars show the standard deviation. Acuity peaks at the fovea and falls smoothly with eccentricity, slightly more steeply in the nasal hemi-retina. The gray line represents the nominal Nyquist limit assuming a crystalline triangular mosaic and cone densities reported by Curcio et al., 1991.

1999; Roorda et al., 2001), but are not distinguishable at the eccentricities with which we are concerned. Fig. 6 shows one of our synthesized mosaics. For each eccentricity represented in the simulation, this array was taken to represent a retinal area that, from the measurements of Curcio et al (1991), would contain 1600 S-cones. These areas ranged in size from 3.0-deg square at the fovea to 6.9-deg square at 20-deg eccentricity. Since our stimulus at the fovea extended into areas of maximal cone density, we assumed the effective foveal cone density to be the average of the peak densities on the principal meridians.

Given a particular mosaic, we present to it either a grating of 93% contrast or blank field, and calculate the signal (assumed to be proportional to quantum catch) arising from each cone. This calculation reflects the actual light levels used during psychophysical testing, and includes the random perturbations expected from quantum fluctuations. Gathering signals from all cones, the model observer's task is to distinguish the spatial distributions of signals that arise under two different conditions (a grating and a blank field of the same mean luminance) and then further to decide whether the grating was vertical or horizontal. Fig. 7 illustrates this process: signals arise from the projection of a 2-deg blank field (A) and a 2 cycle/deg vertical grating (B) onto a synthetic mosaic of S-cones representing 5-deg nasal retina.

Unless a grating has a spatial period smaller than a cone's aperture, the distribution of cone signals elicited in the mosaic will have higher variance than elicited by a spatially uniform field. Similarly, when a vertical grating lies on the mosaic the variance of the distribution of cone signals along any horizontal path will be higher on average than when the grating is horizontal. Panels 7C and 7D show the "horizontal signal" calculated by summing over horizontal slices of the cone array stimulated by a blank field and grating, respectively. The variation within the horizontal signal reflects the amount of horizontal structure in the image. Panels 7E and 7F show the "vertical signal" calculated by summing over vertical slices of the cone array; variation within this signal reflects the amount of vertical structure in the image. To calculate performance, we deliver stimuli as we would in a psychophysical experiment. In each of the two observation intervals in a trial (one containing a vertical grating, the other blank), the model calculates the variance in the quantum catches accumulated along vertical paths and horizontal paths. The horizontal and vertical variances calculated in this way represent all the spatial information about the presence of horizontal and vertical image structure, respectively. A signal-to-noise analysis determines model decisions: for the detection task, the signal (S) is calculated as the sum of the vertical and horizontal variances arising from the grating, while the noise (N) is the sum of variances arising from the blank. The identification decision is similarly computed: since only vertical gratings are presented, the signal comprises the sum of the blank- and grating-induced vertical variances, while the sum of horizontal variances determines the noise. For both tasks, correct decisions are made when the signal-to-noise ratio is greater than unity.

For each of the five synthetic mosaics that we used, and for each eccentricity at which psychophysical measurements had been made, 20 paired presentations of blank fields and gratings were delivered at each of five spatial frequencies spanning four octaves. The size of the stimulus patch was adjusted to match the conditions of psychophysical testing at each eccentricity. To account for small eye movements between fixations, the position of the patch was randomly jittered by up to 10' of arc, and the grating phase randomized, on each presentation. The synthetic psychometric functions were fitted with Weibull curves in the manner done for the psychophysical data, and the threshold acuities derived for each task were averaged across the five mosaics.

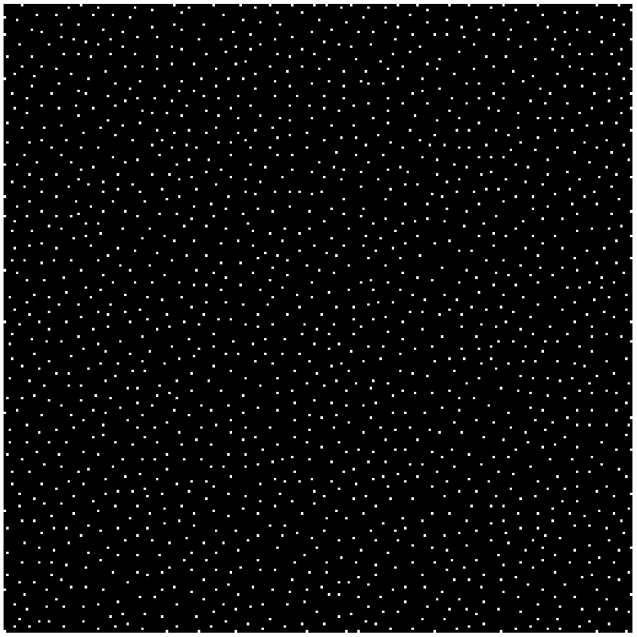

Fig. 6. Array of 1600 S-cones synthesized using the elastic ball model of Shapiro et al. (1985), with the spatial statistics (distances between Voronoi neighbors and central angles of Voronoi regions) of real mosaics. The retinal region represented by the cone array was calculated from Curcio et al.'s (1991) measurements of cone density in the human retina, and ranged from 3 deg square at the fovea to 6.9 deg square at 20-deg eccentricity. Arrays were rendered as 256 × 256 pixel images for manipulation by MatLAB software (MathWorks, Inc.) used for modeling. For each condition in which we were interested, we applied the model observer to five independently generated mosaics, and took the mean estimate of performance.

For all eccentricities, this simple model yielded performance many times higher than that observed in the psychophysical experiments. The model lacks two characteristics of real visual systems that might be expected to limit both detection and identification acuities: it takes no account of noise beyond that due to quantum fluctuations, and it makes no provision for the pooling of S-cone signals at postreceptoral sites.

Noise is introduced by the speckle nature of the coherent light stimulus, and varies with the axial alignment of observers with the interferometer. Neural noise can be assumed to arise beyond the receptors, and can be referred to the source as equivalent input noise (Pelli, 1990). Any pooling of signals from cones will smear the spatial information available to subsequent analysis stages, and will reduce acuity. Such pooling is implied by light- (Kouyama & Marshak, 1992) and electron- (Calkins et al., 1998) microscopic observations of the retinal connections made by S-cones, and by electrophysiological evidence from *in-vitro* recordings made from bistratified ganglion cells that receive inputs from S-cones (Chichilnisky & Baylor, 1999).

To generate realistic thresholds, we provided for two distinct forms of signal degradation: noise added to each cone signal, and pooling of signals beyond the receptors. Noise was incorporated as uniformly distributed perturbations of specified amplitude added to the output of each cone. Pooling was incorporated by convolving the output of the synthetic S-cone array with a blurring kernel of specified diameter, prior to the decision stage.

Because detection acuity varied unsystematically among observers and across eccentricities (presumably due to axial alignment variations and not for interesting physiological reasons), we chose not to seek the additional noise level required to simulate observed detection and identification acuities in each instance. Rather, we sought the level of additional noise required to simulate the observed identification acuities (for which there was good agreement among observers and which varied smoothly as a function of eccentricity), and detection acuities that were about 1.5 times greater—the average difference across all observers and eccentricities.

The form of the pooling filter will depend on the strength and extent of functional connections between cones and bipolar cells, and between bipolar cells and ganglion cells. The available evidence on this (Calkins et al., 1998; Chichilnisky & Baylor, 1999) shows only that an on-center ganglion cell conveying S-cone information receives its principal drive from a single cone, with diminishing contributions from more distant cones. We therefore chose a conical blurring filter for convenience and simplicity . The same general conclusions are reached if the spatial pooling filter has a Gaussian or raised-cosine form.

Fig. 8 shows the effects of variations in noise and pooling on the model's acuity for a vertical grating projected on the cone array. The spatial frequency was 50% greater than the nominal Nyquist limit. Were the image being sampled by a regular mosaic it could not be completely reconstructed. Nonetheless, information about vertical striations is reliably represented. With no added noise beyond quantum fluctuations, and no postreceptoral filter (top left), detection and identification far exceed performance measured psychophysically. From left to right, stochastic noise of increasing amplitude is added to each cone's quantal catch. From top to bottom, a conical postreceptoral blurring filter of increasing diameter has been applied.

The goal was to find the combination of noise level applied globally and blurring filter size adjusted by eccentricity that best characterized the measured detection and orientation identification psychometric functions at each retinal location. Given these constraints, we found only one solution that fitted our results. Each cone's signal was perturbed by a uniformly distributed deviate with amplitude 3.5 times greater than peak quantal catch from the grating. With this level of noise, blurring filter kernel sizes could be found at each retinal location such that the model produced realistic psychometric functions with detection thresholds on average 1.56 times higher than orientation identification thresholds, much like the average of the measured data. Fig. 9 compares modeled and observed acuities for detection and identification. The dashed line shows the average measured detection acuities and the solid line shows the average measured identification acuities for four observers. Open squares and filled circles show, respectively, the average detection and orientation identification acuities obtained by applying the model to five independent synthetic S-cone mosaics. Vertical bars show the standard deviation of five determinations; the variability in the model results is similar to that observed psychophysically.

Fig. 10 shows how the size of the blurring filter required to model the psychophysical data increases with eccentricity. The top panel shows the average number of cones connected by the conical convolution filter at each eccentricity. Near the fovea, convergence of signals from only one or two cones is sufficient to model the results. At retinal locations greater than 10 deg, signals from more than ten cones are required to converge onto postreceptoral elements to reflect the measured data. If we assume that each conical

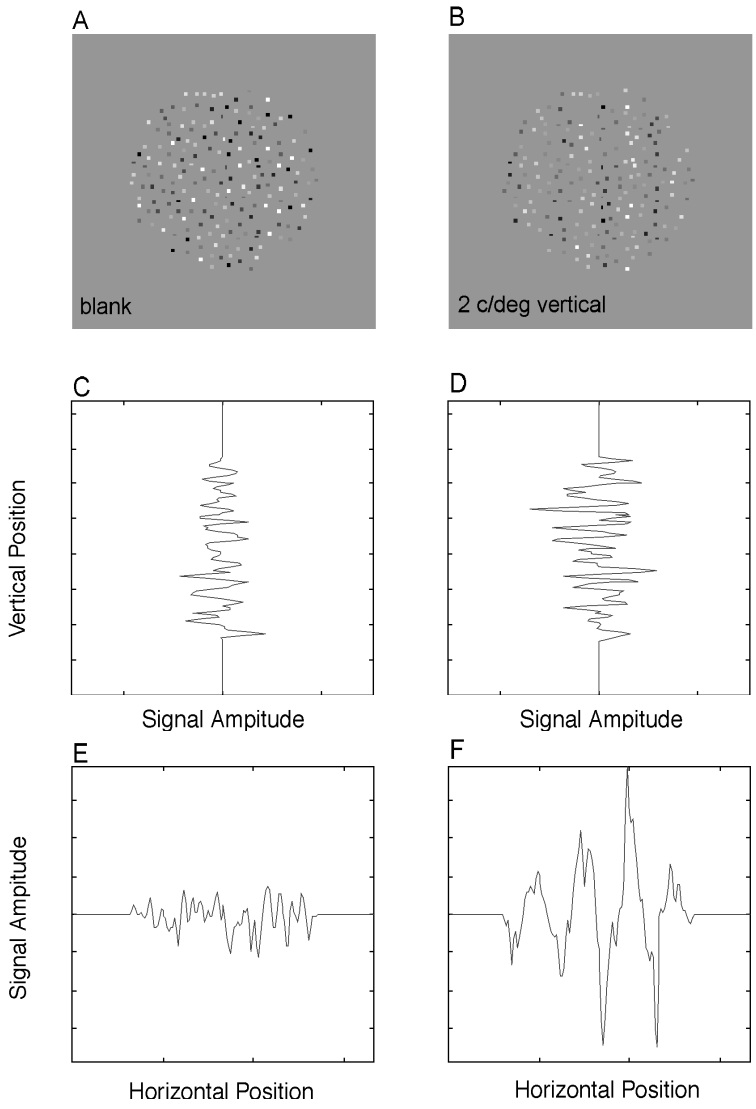

Fig. 7. Modeling detection and identification of gratings. Signals arising from the projection of a 2-deg blank field (A) and a 2 cycle/deg vertical grating with the same average luminance (B) on to a synthesized S-cone mosaic 5 deg in temporal retina. Noise (including that due to quantum fluctuations) is added to the output of each cone. C and D show the average cone signal calculated by summing along horizontal slices of the cone signal array on presentation of a blank field and grating, respectively. The variance of these traces reflects the amount of horizontal structure in the cone signals. E and F show the average cone contrast calculated by summing along vertical slices of the cone signal array. The variance of these traces reflects the amount of vertical structure in the cone signals. In each trial, both the blank field and the grating are presented: the detection decision is based on the sum of the variances arising from the blank versus the grating (i.e. C+E *vs.* D+F) while the orientation identification decision is based on the sum of the horizontal versus vertical variances (i.e. C+D *vs.* E+F).

filter includes a central cone, the bottom panel of Fig. 10 indicates the relative strength of input arising from this central cone. Its proportional contribution falls steadily from almost 100% at the fovea to about 20% at 20-deg eccentricity.

To provide a satisfactory account of the psychophysical results, we need both the added noise and the postreceptoral filter. Adding noise alone made it possible to simulate identification acuities, but in all cases the simulated full psychometric functions (performance *vs.* grating spatial frequency) were unrealistically flat. Moreover, without the postreceptoral filter, the psychometric functions for detection and identification were generally superimposed rather than being separated by a factor of 1.5. Altering the implementation of noise in the model from additive to multiplicative led to no improvement.

Discussion

The foveal identification acuities reported here are consistent with those reported previously. For two of three observers, identification acuity fell slightly faster in nasal than in temporal retina. This might reflect the pronounced naso-temporal asymmetry in S-cone densities found by Curcio et al. (1991). On the assumption that Nyquist frequencies represent limiting acuities, Curcio et al. (1991) concluded, from measurements made by Hess et al. (1989), that the spacing of S-cones limits the resolving power of the S-cone pathway out to 20–30 deg. Our modeling shows that the cone mosaic could support veridical representation of spatial detail well beyond the nominal Nyquist limit, which was what we found in and near the fovea (Fig. 5). For cone arrays that are only slightly less orderly than a regular mosaic, Coletta and Williams (1987) showed that, in the fovea, gratings with spatial frequencies at twice the nominal Nyquist limit will appear as low spatial-frequency aliases at the orthogonal orientation. The psychophysical procedure used here was designed to detect any such orientation reversals, yet none were reliably found. This indicates that, out to 20 deg along the horizontal meridian, the S-cone mosaic is less regular than the foveal L and M mosaics.

Our modeling also shows that at eccentricities greater than 3 deg the mosaic alone could support much better performance than was observed, a fact most readily explained by supposing that

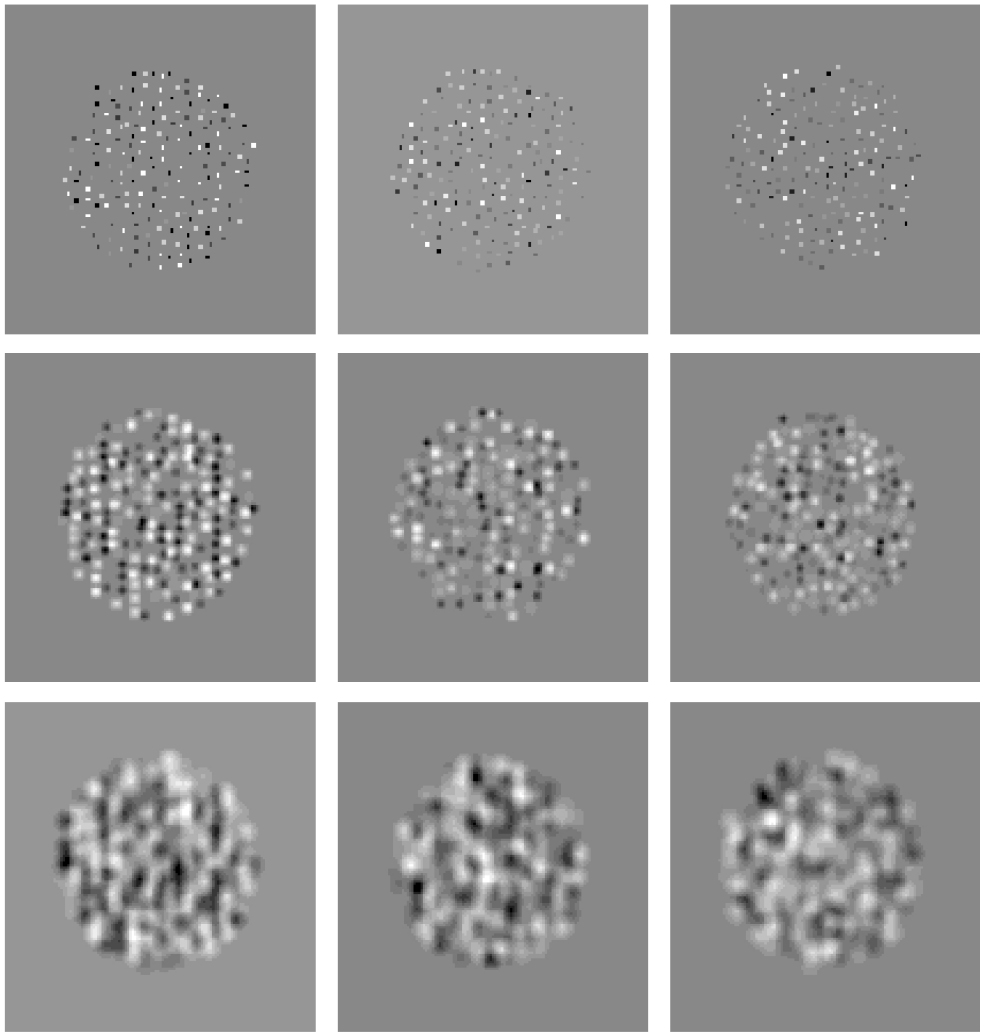

Fig. 8. Illustration of effects of noise and postreceptoral pooling of signals from a vertical grating with spatial frequency 50% greater than the nominal Nyquist limit. Top left panel illustrates signals with no noise (beyond quantum noise) and no pooling. From left to right, increasing amounts of noise are added to the quantal catch of each cone. From top to bottom, a conical blurring filter of increasing diameter has been applied to cone signals. The goal of the modeling was to find a of noise level and filter diameter that best explained psychophysical performance.

cone signals are pooled by postreceptoral mechanisms. The amount of pooling required to account for our observers' performance is consistent with the limited information available from anatomical and physiological measurements. Calkins et al. (1998), using electron-microscopic reconstruction, found that foveal bistratified (blue-on) ganglion cells received the great majority of their inputs from single S-cones, with some additional inputs from a few neighboring cones. *In-vitro* recordings from bistratified ganglion cells in 20-deg to 50-deg retina show that up to 11 cones can drive a single ganglion cell, with one cone typically contributing several times the weight of the others (Chichilnisky & Baylor, 1999).

Given the sparseness of the S-cone mosaic, it is interesting to explore the benefits and costs of pooling cone signals. If the noise in signals from cones in the pool is substantial and uncorrelated, pooling can improve the signal-to-noise ratio for stimuli that extend over the pool, but at the expense of spatial resolving power. To better understand the consequences of pooling, we ran our model to estimate detection and identification performance for 5-deg temporal retina, where the average measured identification acuity is 4.1 cycle/deg. We fixed noise at the value earlier found to be best globally, and varied the sizes of postreceptoral filters. Fig. 11 shows, for gratings of a range of spatial frequencies from 1 cycle/deg to 16 cycle/deg, how the signal-to-noise ratio for identification, averaged over five synthetic mosaics, varied with the size of the pooling filter. Vertical bars show the standard errors of the means. At spatial frequencies below about 2 cycle/deg, increasing the size of the pooling filter leads to progressive gains in signal-to-noise ratio. At higher spatial frequencies nearer the measured acuity (4 cycle/deg), the benefits of increased pooling disappear, but increasing filter size never exacts a substantial penalty because the principal factor limiting performance is the level of noise.

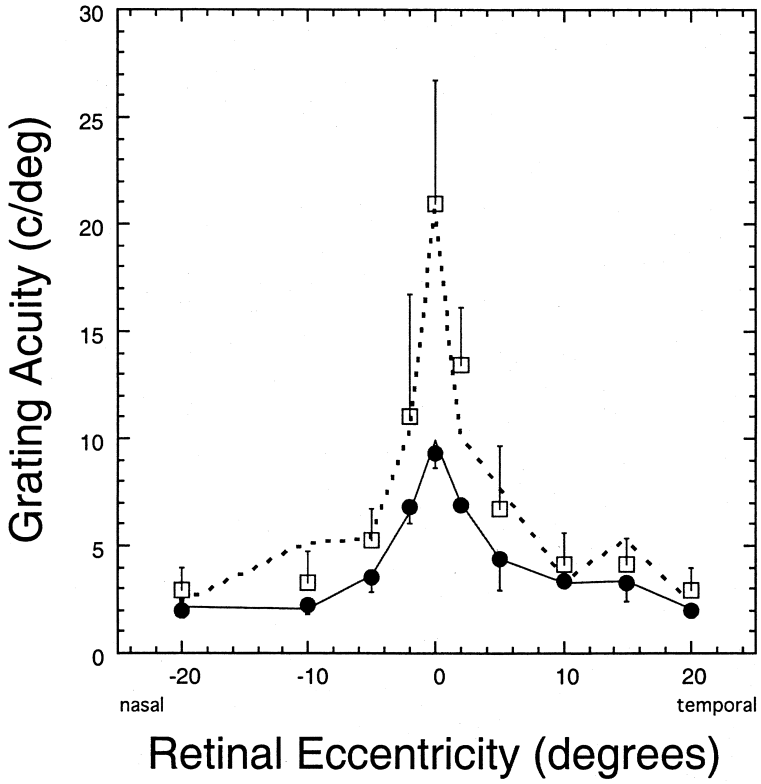

Fig. 9. Modeled detection and orientation identification thresholds as a function of eccentricity. Open squares and filled circles show, respectively, the average detection and identification acuities estimated for five synthetic S-cone mosaics. Vertical bars show one standard deviation. Results were obtained using a fixed amount of added cone noise, and with the size of the postreceptoral blurring filter adjusted to bring performance into line with that measured psychophysically. The dashed line shows the average detection threshold and the solid line shows the average identification thresholds from the psychophysical measurements.

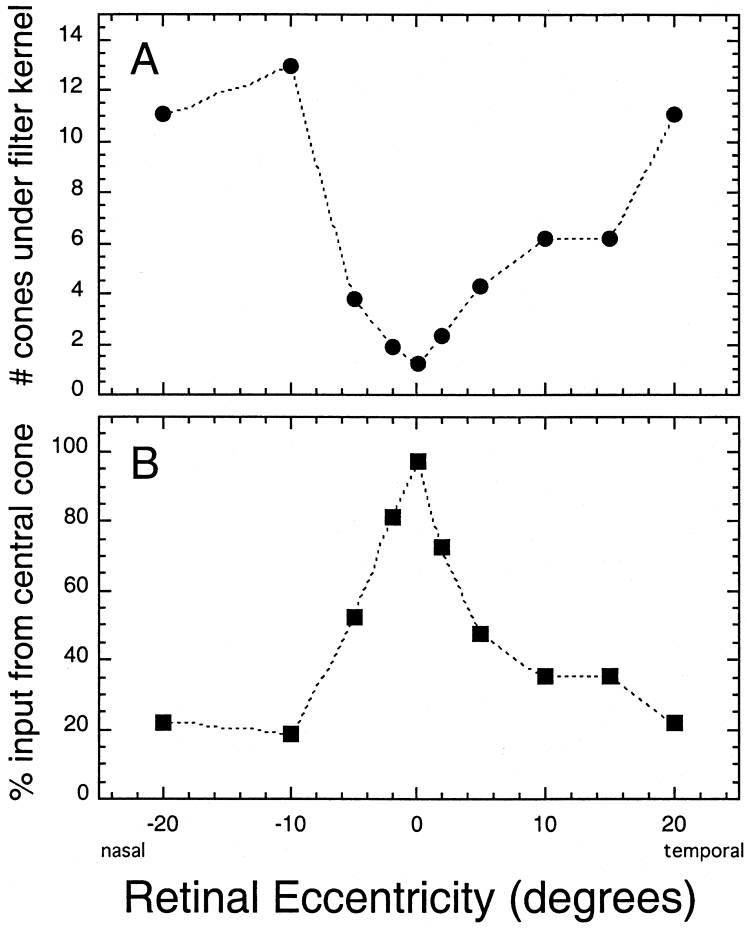

Fig. 10. The size of the conical postreceptoral filter required to characterize psychophysical performance at different eccentricities. A: The average number of cones falling within the filter's diameter at each eccentricity. B: Fraction of total input to the filter provided by the central cone, assuming a cone is present at that position.

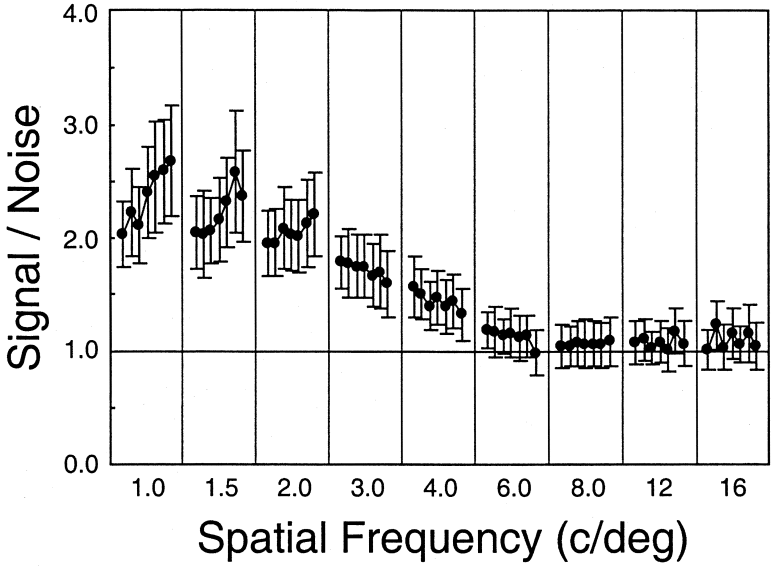

Fig. 11. The effect of spatial pooling on model signal-to-noise ratios for identifying gratings presented to 5-deg temporal retina. Each panel shows the signal-to-noise ratios for a different spatial frequency, noted on the abscissa. From left to right within each panel, the filter diameter increases in 5 μm steps from 49 μm to 79 μm. Average cone spacing in this part of the retina is approximately 31 μm, and the average measured identification acuity 4.1 cycle/deg. Distributions of signal-to-noise ratios were determined by simulating 20 trials at each spatial frequency, for each of five synthetic cone mosaics. Vertical bars show the standard deviations of the average signal-to-noise ratio determined for these mosaics.

Acknowledgments

This work was supported by NIH Grants EY04440, EY01319, and EY13079. We are grateful to David Williams, Nobu Sekiguchi, and David Brainard for allowing us to use their interferometer, and to Walter Makous for advice during the course of the experiments. David Calkins kindly commented on the manuscript.

References

Bumsted, K. & Hendrickson, A. (1999). Distribution and development of short-wavelength cones differ between *macaca* monkey and human fovea. *Journal of Comparative Neurology* **403**, 502–516.

Calkins, D.J., Tsukamoto, Y. & Sterling, P. (1998). Microcircuitry and mosaic of a blue–yellow ganglion cell in the primate retina. *Journal of Neuroscience* **18**, 3373–3385.

Catsano, J.A. & Sperling, H. (1982). Sensitivity of the blue-sensitive cones across the central retina. *Vision Research* **22**, 661–673.

Chichilnisky, E.J. & Baylor, D.A. (1999). Receptive-field microstructure of blue–yellow ganglion cells in primate retina. *Nature Neuroscience* **2**, 889–893.

Coletta, N.J. & Williams, D.R. (1987). Psychophysical estimate of extrafoveal cone spacing. *Journal of the Optical Society of America A* **4**, 1503–1513.

Curcio, C.A., Allen, K.A., Sloan, K.R., Lerea, C.L., Hurley, J.B., Klock, I.B. & Milam, A.H. (1991). Distribution and morphology of human cone photoreceptors stained with anti-blue opsin. *Journal of Comparative Neurology* **312**, 610–624.

Dacey, D.M. & Lee, B.B. (1994). The 'blue-on' opponent pathway in primate retina originates from a distinct bistratified ganglion cell type. *Nature* **367**, 731–735.

de Monasterio, F.M. & Gouras, P. (1975). Functional properties of ganglion cells of the rhesus monkey retina. *Journal of Physiology* (London) **251**, 167–195.

de Monasterio, F.M., McCrane, E.P., Newlander, J.K. & Schein, S.J. (1985). Density profile of blue-sensitive cones along the horizontal meridian of macaque retina. *Investigative Ophthalmology Visual Science* **26**, 289–302.

Derrington, A.M., Krauskopf, J. & Lennie, P. (1984). Chromatic mechanisms in lateral geniculate nucleus of macaque. *Journal of Physiology* (London) **357**, 241–265.

Galli-Resta, L., Novelli, E., Kryger, Z., Jacobs, G.H. & Reese, B.E. (1999). Modelling the mosaic organization of rod and cone photoreceptors with a minimal-spacing rule. *European Journal of Neuroscience* **11**, 1461–1469.

Hess, R.F., Mullen, K.T. & Zrenner, E. (1989). Human photopic vision with only short wavelength cones: Post-receptoral properties. *Journal of Physiology* **417**, 151–172.

Kouyama, N. & Marshak, D.W. (1992). Bipolar cells specific for blue cones in the macaque retina. *Journal of Neuroscience* **12**, 1233–1252.

Macmillan, N.A. & Creelman, C.D. (1991). *Detection Theory: A User's Guide*. Cambridge, England: Cambridge University Press.

McCrane, E.P., de Monasterio, F.M., Schein, S.J. & Caruso, R.C. (1983). Non-fluorescent dye staining of primate blue cones. *Investigative Ophthalmology and Visual Science* **24**, 1449–1455.

Pelli, D.G. (1990). The quantum efficiency of vision. In *Vision: Coding and Efficiency*, ed. Blakemore, C., pp. 3–24. Cambridge: Cambridge University Press.

Roorda, A., Metha, A.B., Lennie, P. & Williams, D.R. (2001). Packing arrangement of the three cone classes in primate retina. *Vision Research* **41**, 1291–1306.

Sekiguchi, N., Williams, D.R. & Brainard, D.H. (1993). Aberration-free measurements of the visibility of isoluminant gratings. *Journal of the Optical Society of America A* **10**, 2105–2117.

Shapiro, M.B., Schein, S.J. & de Monasterio, F.M. (1985). Regularity and structure of the spatial pattern of blue cones of macaque retina. *Journal of the American Statistical Society* **80**, 803–812.

Smith, V.C. & Pokorny, J. (1975). Spectral sensitivity of the foveal cone photopigments between 400 and 500 nm. *Vision Research* **15**, 161–171.

Valberg, A., Lee, B.B. & Tigwell, D.A. (1986). Neurones with strong inhibitory S-cone inputs in the macaque lateral geniculate nucleus. *Vision Research* **26**, 1061–1064.

Wald, G. (1967). Blue blindness in the normal fovea. *Journal of the Optical Society of America* **57**, 1289–1301.

Williams, D. & Collier, R. (1983). Consequences of spatial sampling by a human photoreceptor mosaic. *Science* **221**, 385–387.

Williams, D., Collier, R. & Thompson, B. (1983). Spatial resolution of the short-wavelength system. In *Colour Vision*, ed. Mollon, J. & Sharpe, L., pp. 487–503. New York: Academic Press.

Williams, D.R. (1985*a*). Aliasing in human foveal vision. *Vision Research* **25**, 195–205.

Williams, D.R. (1985*b*). Visibility of interference fringes near the resolution limit. *Journal of the Optical Society of America A* **2**, 1087–1093.

Williams, D.R. & Coletta, N.J. (1987). Cone spacing and the visual resolution limit. *Journal of the Optical Society of America A* **4**, 1514–1523.

Williams, D.R., MacLeod, D.I.A. & Hayhoe, M.M. (1981). Foveal tritanopia. *Vision Research* **21**, 1341–1356.

Willmer, E.N. & Wright, W.D. (1954). Colour sensitivity of the fovea centralis. *Nature* **156**, 119–121.

Yellott, J.I. (1982). Spectral analysis of spatial sampling by photoreceptors: Topological disorder prevents aliasing. *Vision Research* **22**, 1205–1210.